ISSN 1063-7761, Journal of Experimental and Theoretical Physics, 2020, Vol. 130, No. 5, pp. 649–659. © Pleiades Publishing, Inc., 2020.
Russian Text © The Author(s), 2020, published in Zhurnal Eksperimental'noi i Teoreticheskoi Fiziki, 2020, Vol. 157, No. 5, pp. 777–788.

ATOMS, MOLECULES, OPTICS

Peculiarities of Propagation and Amplification of Ultrashort Terahertz Pulses in Strongly Nonequilibrium Plasma Channels Produced in Air by UV Femtosecond Laser Pulses during Multiquantum Ionization

A. V. Bogatskaya[a,b,c,*], E. A. Volkova[a], and A. M. Popov[b,c,d,]**

[a] *Skobeltsyn Research Institute of Nuclear Physics, Moscow State University, Moscow, 119991 Russia*
[b] *Lebedev Physical Institute, Russian Academy of Sciences, Moscow, 119991 Russia*
[c] *Moscow Technical University of Communication and Informatics (MTUCI), Moscow, 111024 Russia*
[d] *Physics Faculty, Moscow State University, Moscow, 119991 Russia*
**e-mail: annabogatskaya@gmail.com*
***e-mail: alexander.m.popov@gmail.com*

Received November 15, 2019; revised December 6, 2019; accepted December 7, 2019

Abstract—The propagation of an ultrashort terahertz (THz) pulse in a nonequilibrium plasma channel produced by a UV femtosecond laser pulse in air is investigated theoretically. The analysis is carried out based on joint solution of the second-order wave equation and the Boltzmann kinetic equation in the binomial approximation for the electron velocity distribution function in the channel plasma. We assume that a THz pulse is quite weak and does not produce a reverse action on the electron energy spectrum in the channel plasma. It is shown that the plasma channel in air under a pressure of several atmospheres is a medium for effective amplification of ultrashort THz pulses in the frequency range up to several terahertz.

DOI: 10.1134/S1063776120040020

1. INTRODUCTION

The interest in effective sources and detectors of radiation in the terahertz frequency range has been rapidly augmented in recent years. This interest is due to unique properties of this radiation that can be of interest in many fundamental and applied problems, in particular, in macromolecular spectroscopy, tomography of biological objects (including applications in medicine), and in safety systems [1–8].

Among various methods and approaches to generation of radiation in the terahertz frequency range, laser generation methods are considered more actively [9–11]. In this case, the action of a high-intensity femtosecond laser pulse from a titanium–sapphire laser and its second harmonic on a gaseous target is considered as a rule [12–15]. One of the mechanisms of terahertz generation in this case is the four-wave mixing process $\Omega = \omega' + \omega'' - 2\omega'''$. Here, ω' and ω'' are the frequencies within the limits of the spectral width of the pulse with frequency ω, and ω''' is the frequency within the limits of the spectral width of a laser pulse with double frequency 2ω. The efficiency of transformation is determined in this case by cubic atomic susceptibility $\chi^{(3)}(\omega' + \omega'' - 2\omega''')$, and the spectral width of the resultant terahertz (THz) signal is in fact determined by the spectral width of the titanium–sapphire laser and its second harmonic. The THz pulse itself is generated only during laser action and has a broad spectrum on the order of the inverse laser pulse duration. For pulses of duration about 100 fs, this value is approximately 10^{13} s^{-1}.

There is also another mechanism of generation of terahertz radiation under a dichromatic laser action on gas media. This mechanism is associated with asymmetry of emission of photoelectrons in the radiation field polarization direction (both field components are assumed to be polarized linearly in the same direction) during the ionization of an atom in a strong dichromatic field; as a result, low-frequency plasma oscillations appear by the end of the laser pulse in the resultant plasma formation [11, 16–18]. The frequency of these oscillations is determined by the electron concentration in the resultant plasma formation and by its shape. For example, for a spherical plasma formation (this case approximately corresponds to sharp focusing of the laser beam), the plasma resonance frequency is $\Omega = \omega_p/\sqrt{3}$ (here, $\omega_p = \sqrt{4\pi e^2 n_e/m}$ is the plasma frequency and n_e is the electron concentration). In the case of focusing of radiation by a long-focal-length lens, the shape of the plasma formation

can be approximated by a prolate ellipsoid; in this case, $\Omega \approx \omega_p/\sqrt{2}$ [19]. For electron concentrations $n_e \geq 10^{15}$–10^{16} cm^{-3}, the corresponding frequencies fall into the terahertz interval. The terahertz pulse duration in this case is determined by the rate of damping of plasma oscillations, i.e., by the frequency of electron–atom (or ionic) collisions. At gas pressures close to the atmospheric pressure, this frequency is only slightly lower than resonance frequency Ω. As a result, the radiation spectral width is also on the order of the carrier frequency, and a THz pulse is found to be short (one–two or several periods of oscillations).

Because of significant difference between the generation mechanisms considered here, the excitation of plasma oscillations in a plasma necessitates the action of much stronger optical fields since a considerable ionization of gas is required, while the four-wave mixing process occurs on neutral (unionized) atoms/molecules of the medium. In both cases, however, the efficiency of conversion of optical radiation into the terahertz range is low, as a rule, and amounts to $\sim 10^{-4}$–10^{-6} [20–24]. In such a situation, the elevation of efficiency of conversion of optical radiation into terahertz radiation is a topical problem.

On the other hand, a method of amplification of subterahertz radiation in strongly nonequilibrium plasma channels formed in a gas as a result of its multiphoton ionization by a UV femtosecond laser pulse was proposed in [25]. The necessary condition for amplifying radiation with frequency $\omega < \nu_{tr}$ (ν_{tr} is the transport frequency of electron–atom collisions in a plasma channel) is a rapidly increasing transport scattering cross section $\sigma_{tr}(\varepsilon)$ with increasing energy in the region of formation of a photoelectron peak in the electron spectrum:

$$\frac{d}{d\varepsilon}(\varepsilon/\sigma_{tr}(\varepsilon)) > 0. \quad (1)$$

Such a situation is realized, for example, for the three-photon ionization of xenon by radiation from the KrF excimer laser with photon energy of 5 eV [25]. The ionization potential of the xenon atom is 12.13 eV; therefore, during its ionization, the photoelectron spectrum in the energy range of about 2.87 eV acquires a peak, and the Ramsauer minimum on the transport scattering cross section ensures the fulfillment of condition (1). Such a form of the electron energy distribution function (EEDF), in fact, indicates the existence of an energy interval characterized by inversion in the continuum, which ultimately ensures the amplification effect [26, 27]. On the other hand, the amplification effect in question is close in nature to the absolute negative conductivity of the gas, which was predicted long ago [28] and was observed experimentally in [29]. Under the atmospheric pressure of the gas (xenon), quantity $\sigma_{tr}(\varepsilon = 2.87\ \text{eV}) \approx 1.5 \times 10^{-15}$ cm^{-2} in the region of formation of the photoionization peak, which ensures amplification in the subterahertz frequency range over time intervals up to a few dozen nanoseconds [25]. The efficiency of amplification can be quite high: according to estimates [30], several percent of the energy stored in the channel can be converted into the energy of the THz pulse. An increase in the gas pressure accelerates relaxation of nonequilibrium (spiking) energy distribution and reduces the duration of the observed inversion effect, thus ensuring amplification of radiation at higher frequencies in the terahertz range. As noted above, the existing laser methods of THz generation make it possible as a rule to obtain pulses of duration of one–two periods of oscillations (see also [18, 31, 32]). Therefore, for radiation frequency $\Omega = 5 \times 10^{12}$ s^{-1}, it is sufficient to preserve the amplifying properties of the medium for 1–2 ps. As a result, a combined source of THz radiation was proposed [33], in which the initial pulse was generated due to the action of the dichromatic laser field on a gaseous medium; then this pulse was multiplied in the nonequilibrium plasma channel in accordance with the mechanism described above. Theoretically, it may happen that one of the laser pulses producing the initial signal can be used for the formation of the nonequilibrium channel.

It was shown in [34] that the regime of amplification of rf laser pulses can also be realized in plasma channels produced by a UV femtosecond laser pulse in nitrogen or in air. This effect is also based on the increase in the transport cross section in nitrogen in energy range 1.5–2.2 eV (Fig. 1). However, the existence of low vibrational states of the nitrogen molecule, which lead to a much faster relaxation of the electron energy spectrum in nitrogen (air) as compared to its relaxation in rare gases, is significant in this case. The energy dependences of the excitation cross section for two lower vibrational states of the nitrogen molecule are shown in Fig. 2. (The data for required cross sections of electron scattering by nitrogen and oxygen molecules can be found in [35, 36].)

It can be seen that the cross sections are characterized by a sharp peak near 2 eV. To avoid rapid degradation of the energy peak in the photoelectron spectrum, it is important to choose its position in energy range 1.7–1.9 eV. Such an initial position of the photoelectron peak can be obtained in air as a result of three-photon ionization of the oxygen molecule (ionization potential is 12.08 eV) by the third harmonic of the titanium–sapphire laser [34]. However, the duration of the amplification regime under the atmospheric pressure also does not exceed 20 ps in this case [34]. In fact, this means that only extremely short terahertz pulses with durations of a few periods of field oscillation can be amplified in air (nitrogen). At the same time, analysis of the Boltzmann kinetic equation was performed in aforementioned publications [30, 34] for a quasi-monochromatic rf radiation. Such an approach is not applicable for analyzing the response of a plasma medium to extremely short electromagnetic pulses, because of the strong dependence of the

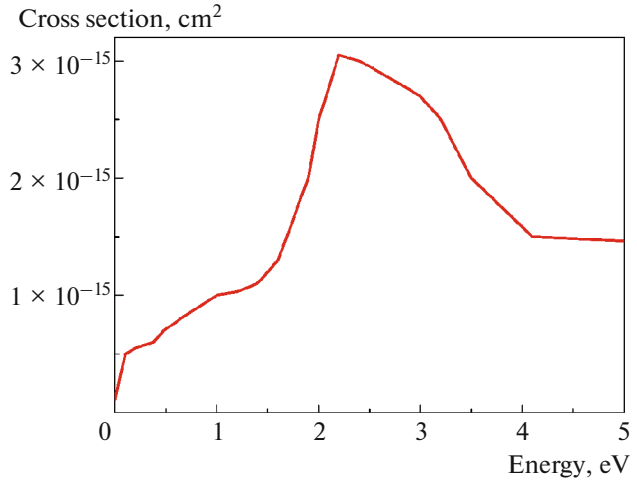

Fig. 1. (Color online) Transport cross section of electron scattering by nitrogen molecules.

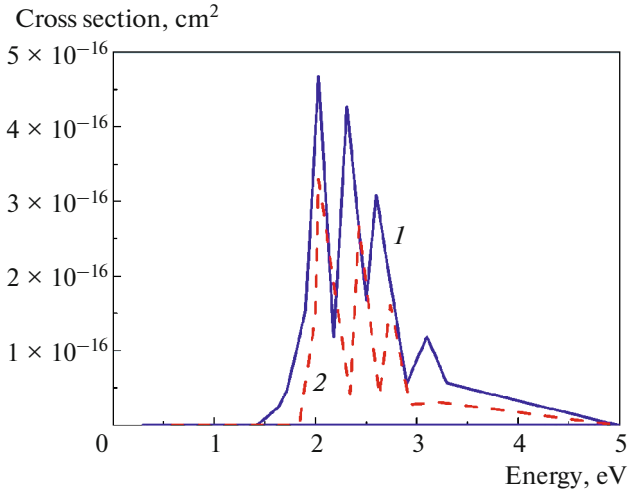

Fig. 2. (Color online) Vibrational excitation cross section for two lower states of the nitrogen molecule.

spectral function of the electron gas response on the radiation frequency. On the other hand, the possibility of using the parabolic approximation for analyzing the propagation of ultrashort pulses is also doubtful. For this reason, we are using in this study a self-consistent approach based on the solution of the second-order wave equation for a THz pulse propagating in a plasma, the response function for which is calculated for a strongly nonmonochromatic pulse in the conditions of the electron energy distribution rapidly relaxing in time. The analysis performed here demonstrates the possibility of effective amplification of ultrashort THz radiation pulses in air plasma under a pressure of several atmospheres. The amplification process in this case is accompanied with a noticeable distortion of the spectral composition of the signal, which leads among other things to tailing of signal at the exit of the amplifying medium.

2. RESPONSE OF THE PLASMA FORMATION TO AN EXTERNAL ELECTROMAGNETIC FIELD

In analysis of the response of a plasma formation produced by an intense UV femtosecond laser pulse to an external THz field, we proceed from the Boltzmann kinetic equation for the electron velocity distribution function (EVDF) in the channel [37]:

$$\frac{\partial f(\mathbf{v},t)}{\partial t} - \frac{e\mathbf{E}(t)}{m}\frac{\partial f}{\partial \mathbf{v}} = \mathrm{St}(f), \qquad (2)$$

where $\mathbf{E}(t)$ is the electric field of the THz pulse propagating in the channel, $\mathrm{St}(f)$ is the collision integral describing the EVDF variation in elastic and inelastic collisions, and the distribution function itself is normalized as $\int f(\mathbf{v},t)\, d^3\mathrm{v} = 1$. In the case of the linear polarization of the THz pulse, it is convenient to analyze Eq. (2) using polynomial expansion

$$f(\mathbf{v},t) = \sum_{\ell} f_{\ell}(\mathrm{v},t)P_{\ell}(\cos\theta), \qquad (3)$$

where $P_{\ell}(\cos\theta)$ is the Legendre polynomial and θ is the angle between the electron velocity vector and the electric field vector of the wave (z axis). We can easily show that the current induced in the plasma by electric field $E(t)$ is also directed along the z axis and can be expressed in terms of the first angular harmonic of polynomial expansion

$$j(t) = -\frac{4\pi}{3} en_e \int \mathrm{v}^3 f_1(\mathrm{v},t)d\mathrm{v}. \qquad (4)$$

In the case of weak EVDF anisotropy (which can be induced by the acting field or determined by the initial distribution function), it is sufficient to retain only the first two harmonics in expansion (3):

$$f(\mathbf{v},t) = f_0(\mathrm{v},t) + f_1(\mathrm{v},t)\cos\theta. \qquad (5)$$

In this case, the equation for $f_1(\mathrm{v}, t)$ can be written in form

$$\frac{\partial f_1(\mathrm{v},t)}{\partial t} + \nu_{\mathrm{tr}}(\mathrm{v})f_1(\mathrm{v},t) = \frac{eE(t)}{m}\frac{\partial f_0}{\partial \mathrm{v}}, \qquad (6)$$

where ν_{tr} is the transport scattering frequency. For example, ν_{tr} for air is the sum of the partial transport frequencies of scattering by nitrogen and oxygen molecules:

$$\nu_{\mathrm{tr}} = \nu_{\mathrm{tr}}^{\mathrm{N}} + \nu_{\mathrm{tr}}^{\mathrm{O}} = \nu N(\alpha\sigma_{\mathrm{tr}}^{\mathrm{N}} + (1-\alpha)\sigma_{\mathrm{tr}}^{\mathrm{O}}). \qquad (7)$$

Here, N is the total concentration of molecules in the gas, $\alpha \approx 0.79$ is the partial fraction of nitrogen molecules in air, and $\sigma_{\mathrm{tr}}^{\mathrm{N}}$ and $\sigma_{\mathrm{tr}}^{\mathrm{O}}$ are the transport scattering cross sections for nitrogen and oxygen molecules,

respectively (these cross sections were taken from [35, 36]).

As regards zeroth distribution function harmonic $f_0(\nu, t)$, its time evolution is described by equation

$$\frac{\partial f_0(\nu,t)}{\partial t} = \frac{eE(t)}{3m\nu^2}\frac{\partial}{\partial \nu}(\nu^2 f_1(\nu,t)) + Q_{el}(f_0) + Q^*(f_0) + Q_{ee}(f_0). \quad (8)$$

The first term of this equation describes the heating of the electron gas by the wave field, while the second, third, and fourth terms are the integrals of elastic, inelastic, and electron–electron collisions, respectively. The elastic collision integral can be written as [37]

$$Q_{el}(f_0) = -\frac{1}{\nu^2}\frac{\partial}{\partial \nu}\left(\nu^2 \nu_{\text{eff}}\left(\nu f_0(\nu,t) + \frac{T_g}{m}\frac{\partial f_0}{\partial \nu}\right)\right). \quad (9)$$

Here,

$$\nu_{\text{eff}} = \frac{m}{M_N}\nu_{tr}^N(\nu) + \frac{m}{M_O}\nu_{tr}^O(\nu)$$

is the effective energy loss frequency; M_N and M_O are the molecular masses of nitrogen and oxygen, respectively; ν_{tr}^N and ν_{tr}^O are the corresponding partial transport frequencies, and T_g is the gas temperature. Among inelastic processes occurring in the given case, the excitation of vibrational states of the nitrogen molecule is the most significant process (see [34] for details). As regards the electron–electron collisions, the corresponding integral was considered in [37]. The predominance of these collisions leads to Maxwellization of the electron spectrum. It was shown in [38] that the effect of the electron–electron collisions on the form of the energy spectrum at atmospheric pressure can be ignored (at least, up to concentration $n_e = 10^{14}$ cm^{-3}).

We assume that by the instant of propagation of a terahertz pulse through the plasma channel, the isotropic electron velocity distribution determined by three-photon ionization of oxygen molecules by the third-harmonic radiation of the Ti–Sa laser ($\hbar\omega = 4.65$ eV) has been formed in the channel. In this case, the photoelectron peak corresponds to energy $\langle\varepsilon\rangle = 1.87$ eV. We approximate the photoelectron peak a Gausian shape of width $\Delta\varepsilon = 0.1$ eV centered near $\langle\varepsilon\rangle$:

$$f_0(\nu) = \frac{1}{4\pi}\frac{m^{3/2}}{\Delta\varepsilon\sqrt{2\pi(m\nu^2/2)}} \times \exp\left(-\frac{(m\nu^2/2 - \langle\varepsilon\rangle)^2}{(\Delta\varepsilon)^2}\right). \quad (10)$$

Such an EVDF is equivalent to the initial electron energy distribution used in [34].

The angular distribution of photoelectrons requires a more detailed analysis. In the case of multiphoton ionization of nitrogen or oxygen molecules with an arbitrary orientation of molecular axes, this distribution is obviously not strictly isotropic and should be considered specially. However, this distribution becomes isotropic quite soon over times on the order of the inverse transport frequency; in the conditions considered below, this time does not exceed 100 fs and turns out to be comparable with the duration of the ionizing UV pulse.

The general solution to Eq. (6) for given zeroth harmonic $f_0(\nu, t)$ of arbitrary function $E(t)$ and initial condition $f_1(\nu, t \to \infty) = 0$ (i.e., the initial velocity distribution is isotropic) can be written as

$$f_1(\nu, t \to -\infty) = \frac{e}{m}\exp(-\nu_{tr}(\nu)t) \times \int_{-\infty}^{t} \exp(\nu_{tr}(\nu)t')E(t')\frac{\partial f_0(\nu,t')}{\partial \nu}dt'. \quad (11)$$

Substituting this solution into expression (4) for the current induced in the plasma by a terahertz pulse, we obtain (see [39])

$$j(t) = \int_0^t \sigma(\tau, t-\tau)E(t-\tau)d\tau, \quad (12)$$

where the response function is given by

$$\sigma(\tau, t-\tau) = \frac{4\pi e^2 n_e}{3m} \times \int \nu^3\left(-\frac{\partial f_0(\nu, t-\tau)}{\partial \nu}\right)\exp(-\nu_{tr}(\nu)\tau)d\nu. \quad (13)$$

In this case, zeroth harmonic $f_0(\nu, t - \tau)$ is determined from the solution to Eq. (8) and in the general case is also a function of the electric field strength of the wave. This means that the relation between the current density and field (12) is nonlinear, and the spectrum of the propagating pulse actually acquires frequencies that are absent in the initial pulse. However, in the case of weak pulses being amplified, the effect of the electric field of the wave on the time evolution of $f_0(\nu, t)$ can be disregarded assuming that spectrum relaxation is determined only by elastic, inelastic, and electron–electron collisions. In this study, we confine our analysis to precisely this case. According to estimates [34], such a situation is realized at least up to the THz field intensity on the order of 10^3 W/cm^2. At higher values of intensity of THz radiation, additional diffusion broadening of the photoelectron peak in the energy space lowers the efficiency of amplification in the channel.

It can be seen that expressions (12) and (13) demonstrate the retardation effect; the current in the plasma is determined by the electric field, including that at the previous instants, but the "retardation depth" is determined in this case by the inverse transport frequency, which is different for different electron velocities. In addition, the response function is also determined by the electron velocity distribution func-

tion at the retardation instant. The retardation effect is obviously especially important in analysis of propagation of extremely short pulses in gases in which fast time evolution of the EVDF occurs.

Integrating expression (13) by parts and considering the normalization condition, we obtain

$$\sigma(\tau, t-\tau) = \frac{4\pi e^2 n_e}{m}\int \nu^2 f_0(\nu, t-\tau) \times\left(1-\frac{\nu\tau}{3}\frac{dv_{\rm tr}(\nu)}{\partial\nu}\right)\exp(-v_{\rm tr}(\nu)\tau)d\nu. \quad (14)$$

It is clear from the physical meaning of the response retardation effect that the response function is determined only for a positive value of argument $t-\tau>0$, while for a negative value of the second argument ($t-\tau<0$), we must assume that the response function turns to zero.

The above expression written in such a form demonstrates the possibility of electromagnetic field amplification effect in the plasma. Indeed, for the transport scattering cross section increasing with velocity, the expression in the parentheses in Eq. (14) can make a negative contribution to the integral; the response function can become negative, and the negative absorption effect (i.e., amplification of the electromagnetic wave in the plasma) can appear if it is this velocity interval that makes a decisive contribution to integral (14). It is significant that the amplification effect also depends on the existence of retardation because the current induced in the plasma is a nonlocal function of the field. Detailed analysis of the response function for the nitrogen plasma and the spiking velocity distribution function in form (10) was performed in [39].

3. NUMERICAL MODEL

Let us briefly consider the numerical model that was used in analysis of the propagation in the plasma of the THz pulse in the conditions of fast variation of the EVDF. We assume that an ionizing femtosecond pulse producing a spatial region in which the amplification of a terahertz signal is possible propagates over the gas with the velocity of light. The size of this region is determined by the EVDF relaxation rate. Precisely in this amplification region, the THz radiation pulse must propagate (Fig. 3). It should also be noted that simultaneously with the regime of rf radiation amplification, a waveguide regime can appear in the channel [38], because the refractive index of the nonequilibrium plasma is greater than unity; i.e., the plasma turns out to be an optically denser medium as compared to the unionized gas [40]. The length of the waveguide region turns out to be larger than the length of the amplification zone.

On the other hand, the diffraction length for the transverse size of the THz radiation beam of a few millimeters for the THz radiation of frequency 10^{13} s^{-1} is approximately 30 cm. At qualitative level, this allows us to confine our analysis of the problem to the second-order 1D wave equation

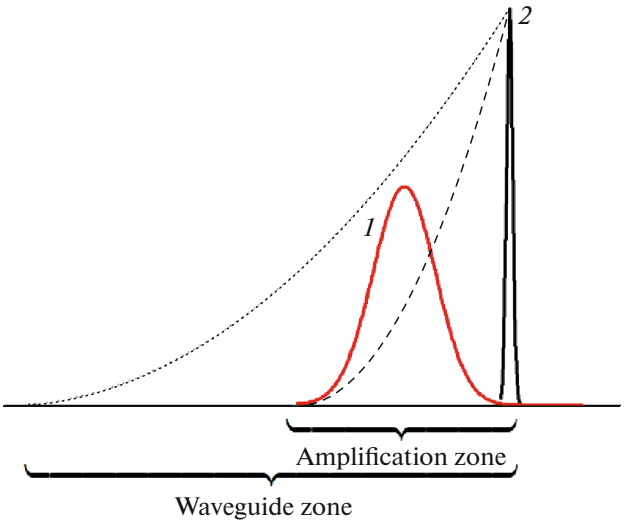

Fig. 3. (Color online) Schematic diagram of a THz pulse (*1*) propagating in a waveguide channel produced by a UV laser pulse (*2*). Dotted and dashed curves show the waveguide and amplification zones of the THz signal.

$$\frac{\partial^2 E(x,t)}{\partial x^2} = \frac{1}{c^2}\frac{\partial^2 E(x,t)}{\partial t^2} + \frac{4\pi}{c^2}\frac{\partial j(x,t)}{\partial t}, \quad (15)$$

where the current density in the plasma is connected with the electric field by relation

$$j(x,t) = \int_0^t \sigma(\tau, t-x/c-\tau)E(x,t-\tau)d\tau, \quad (16)$$

and the response function is defined by expression (14), but depends on retarded argument $t-x/c$, which corresponds to the formation of the photoionization plasma in a femtosecond UV pulse propagating in the positive direction of the x axis with the velocity of light. In fact, the retarded argument indicates that the EVDF determining response function (14) is different at different spatial points of the channel, because the time of its relaxation at a given spatial point is $t-x/c$. In this case, the response function is zero in region $t-x/c-\tau<0$.

While choosing the initial conditions ($t=0$) for Eq. (15), we assume that the femtosecond pulse is at the point with coordinate $x=0$, and the initial THz pulse that has already been formed is in the unionized gas (vacuum) in the region of negative values of the coordinate. It is convenient to define this pulse in terms of vector potential

$$A(\xi\in(-\ell,0))|_{t=0} = A_0\left(\sin^5\left(\pi\frac{\xi-\ell}{\ell}\right)\sin\left(2\pi\frac{\xi-\ell}{\ell}\right)\right). \quad (17)$$

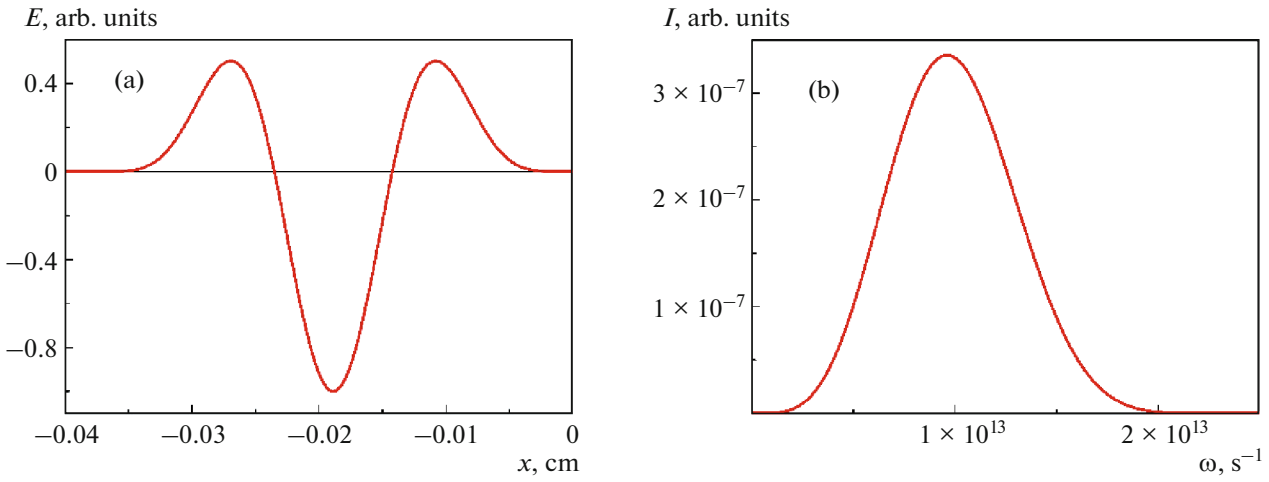

Fig. 4. (Color online) (a) Initial THz radiation pulse and (b) its spectral composition.

Here, $\xi = x - ct$ and $\ell = 0.038$ cm is the length of the pulse in space. Outside this interval $(-\ell, 0)$, the vector potential is set at zero. In this case, the initial values of the electric field and its time derivative are determined by single and double differentiation of expression (17) with respect to time. In particular, for the initial field distribution, we obtain

$$E(x \in (-\ell,0), t = 0) = E_0\left(\sin^5\left(\pi\frac{x-\ell}{\ell}\right)\cos\left(2\pi\frac{x-\ell}{\ell}\right) + \frac{5}{2}\sin^4\left(\pi\frac{x-\ell}{\ell}\right)\cos\left(\pi\frac{x-\ell}{\ell}\right)\sin\left(2\pi\frac{x-\ell}{\ell}\right)\right). \quad (18)$$

Here, $E_0 = 2\pi A_0/\ell$.

The pulse defined in form (17), (18) is a single-cycle pulse, and condition $\int E(x)dx = 0$ is satisfied. The fulfillment of this condition indicates the absence of the static field component of the laser pulse. The pulse itself has duration $\tau = \ell/c \approx 1.26 \times 10^{-12}$ s and is in the region of negative values of the coordinate (Fig. 4a), while point $x = 0$ corresponds to the leading edge of the pulse.

The spectral composition of the THz pulse defined by relation (18),

$$I_{k=\omega/c} \sim \left|\int E(x, t = 0)\exp(ikx)dx\right|^2, \quad (19)$$

is shown in Fig. 4b. It can be seen that the pulse considered here is indeed characterized by a broad radiation spectrum with frequencies varying in fact from zero to 20 THz; the spectral intensity peak approximately corresponds to a frequency of 10^{13} s^{-1}. In such a situation, the low-frequency part of this spectrum can be amplified; conversely, the high-frequency part can be absorbed (see [38]). As a result, the pulse is considerably distorted and tailed.

The method of numerical solution of second-order wave equation (15) was considered in [41]. The time integration step was $\Delta t = 4.8834 \times 10^{-16}$ s. The spatial discretization step was $\Delta x = c\Delta t \approx 1.465 \times 10^{-5}$ cm. The length of the spatial countable domain was 0.12–0.24 cm depending in the conditions of the problem. The equation was integrated in such conditions that the countable domain boundaries were remote.

4. DISCUSSION

Let us begin our analysis with the evolution of the electron distribution function in the air plasma produced by the third harmonic of the Ti–Sa laser. As noted above, in the case of low intensities of the THz pulse being amplified, this evolution is determined primarily by the excitation of the vibrational degree of freedom of nitrogen molecules by photoelectrons and is considered in detail in [34]. Calculations show that under the atmospheric pressure, the inverse effect of the amplified field on the electron energy spectrum in the channel plasma can be ignored up to intensities of 10^3 W/cm^2 over times of up to 20 ps. As regards the electron–electron collisions, their effect in the air (nitrogen) plasma under the atmospheric pressure is insignificant at least for $n_e \le 10^{14}$ cm^{-3} [38].

For our analysis, it is most important that for the initial position of the photoelectron peak near 1.8 eV, the initial shape of the energy distribution is approximately preserves during its time evolution [34], while the peak as a whole is shifted towards lower energies due to the energy loss for vibrational excitation of nitrogen molecules. Depending on the distance from the femtosecond laser pulse propagating in the gas with the velocity of light and producing the channel

plasma, the energy position of photoelectron peak $\langle\varepsilon(x)\rangle$ can be approximately described by equation

$$\frac{d\langle\varepsilon\rangle}{dx} = -cv_{\nu}^{*}(\langle\varepsilon\rangle)I_{\nu}, \qquad (20)$$

where v_{ν}^{*} is the frequency of excitation of the vibrational state of the nitrogen molecule and $I_{\nu} = 0.29$ eV is the vibrational quantum of the nitrogen molecule. As regards elastic collisions with nitrogen or oxygen molecules, the fraction of energy lost by an electron in an elastic collision is ~$(2m/M)\varepsilon$ (M is the mass of the nitrogen or oxygen molecule), which renders energy loss in elastic collisions negligibly low as compared to the energy loss in vibrational excitations. The solutions to Eq. (20) for different molecular concentrations N are shown in Fig. 5. The result depicted in Fig. 5 show that the size of the amplification zone (corresponding to the position of the photoionization peak in region $\langle\varepsilon\rangle \geq 1.5$ eV) is not smaller than 0.1 cm in all cases, which is much larger than the length of the pulse considered here. As regards the electron–electron collisions, they lead to diffusion broadening of the photoelectron peak. However, the estimates obtained in [34, 38] show that in the conditions of our calculations, for $n_e \leq 10^{14}$ cm^{-3}, the effect of these collisions on the form of the electron energy distribution can be ignored.

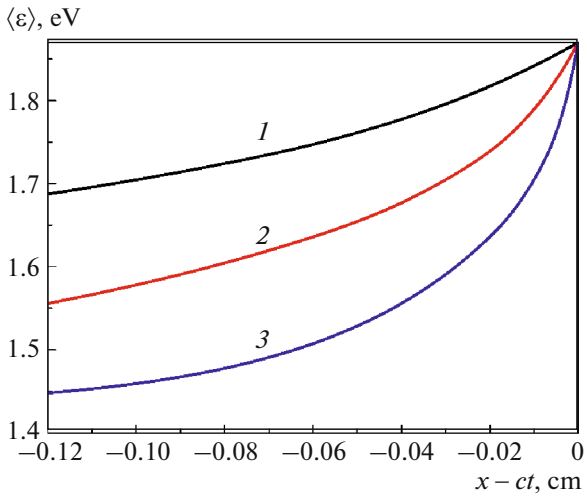

Fig. 5. (Color online) Distribution of the mean energy of the photoelectron peak along the plasma channel formed during ionization of air by the third harmonic of the Ti–Sa laser for different concentrations $N = 3 \times 10^{19}$ (*1*), 10^{20} (*2*), and 3×10^{20} cm^{-3} (*3*). The femtosecond laser pulse forming the plasma channel is at the point with coordinate $x = 0$.

Let us now consider the results of the solution of wave equation (15) with the response function in form (16) and initial condition (17). Figure 6 shows the evolution of a THz radiation pulse and its spectral composition for gas concentration $N = 10^{20}$ cm^{-3} and electron concentration $n_e = 3 \times 10^{13}$ cm^{-3}. The calculated data (Fig. 6a) are given in coordinates "attached" to the femtosecond laser pulse forming the plasma, located at the spatial point with coordinate $x = 0$, and propagating with the velocity of light. Calculations show that indeed the high-frequency part of the pulse spectrum is absorbed, while the low-frequency part is amplified. The boundary frequency separating the regions of signal absorption and amplification is found to be approximately 7×10^{12} s^{-1}, which is close to the central frequency of the THz pulse and approximately corresponds to frequency $\omega^* \approx \nu_{tr}/2$ [38], where the transport frequency was taken for electron energy of 1.87 eV. The narrowing of the spectrum of the pulse being amplified and the change of its central frequency to approximately 3×10^{12} s^{-1} lead to a noticeable increase in its duration.

A different situation is realized for $N = 3 \times 10^{20}$ cm^{-3} and $n_e = 3 \times 10^{13}$ cm^{-3} (Fig. 7). An increase in the gas pressure leads to an increase in the critical frequency separating the regions of absorption and amplification of the THz signal. As a result, almost the entire spectral composition of the pulse falls into the amplification zone. In this case, an increase in the transport frequency leads to a decrease in the "memory depth" of the system (see expression (14) for the system response). In such a situation, elementary analysis of expression (14) for the response function shows that an increase in the molecular (atomic) concentration of the medium leads to a decrease in the absolute value of quantity σ and, hence, to the reduction of the amplification factor.

On the other hand, a decrease in the gas pressure leads to a decrease in critical frequency ω^* separating the THz signal amplification and absorption regions. Such a regime of pulse propagation for $N = 3 \times 10^{19}$ cm^{-3} and $n_e = 3 \times 10^{13}$ cm^{-3} is shown in Fig. 8. In this case, $\omega^* \approx 2.5 \times 10^{13}$ s^{-1}, and the major part of the initial pulse is absorbed except for its low-frequency component. However, for large lengths of propagation of radiation in the channel, the amplification of the low-frequency part of the THz pulse becomes noticeable, and the peak of its spectral intensity is near 10^{12} s^{-1}. This frequency value corresponds to a wavelength of about 0.2 cm, which is several times larger than the length of the initial pulse. For this reason, a "tail" lagging more and more behind the UV laser pulse is formed during its propagation and absorption in the channel of the initial THz pulse and during amplification of its low-frequency part (see Fig. 8). As a result, a new low-frequency single-cycle pulse of the aforementioned length is formed (see Fig. 8).

As regards the dependence of the amplification effect on the electron concentration in the plasma channel, in the absence of electron–electron collisions, the amplification (absorption) of the THz signal turns out to be proportional to the electron number density.

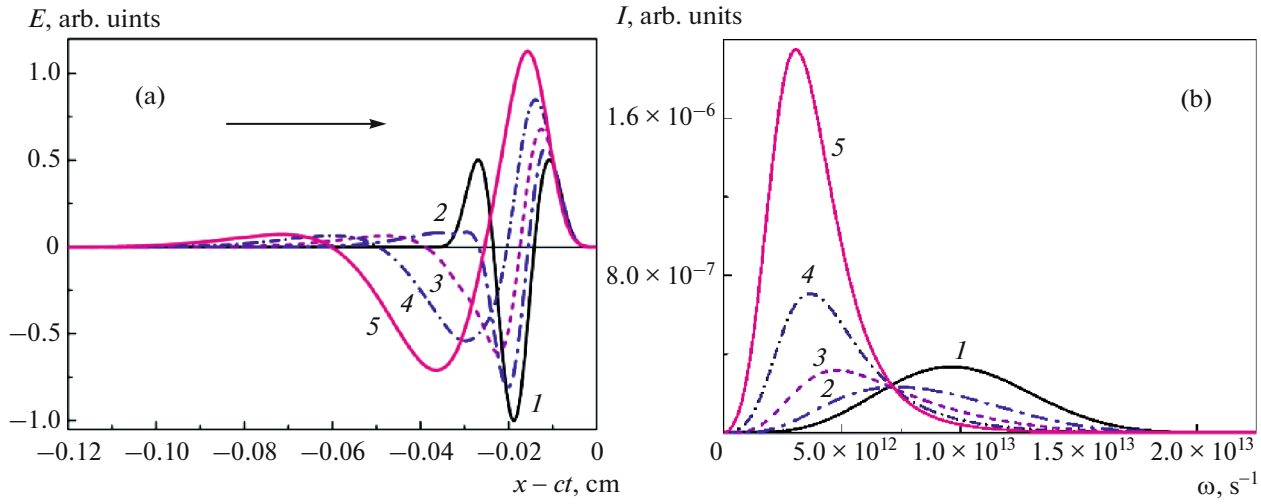

Fig. 6. (Color online) Evolution of (a) a THz pulse and (b) its central composition. The electron concentration in the plasma channel is $n_e = 3 \times 10^{13}$ cm^{-3} and the concentration of neutral particles is $N = 10^{20}$ cm^{-3}. Arrow indicates the THz pulse propagation direction. The curves correspond to different instants: 0 (*1*), 0.25 (*2*), 0.5 (*3*), 0.75 (*4*), and 1 ns (*5*).

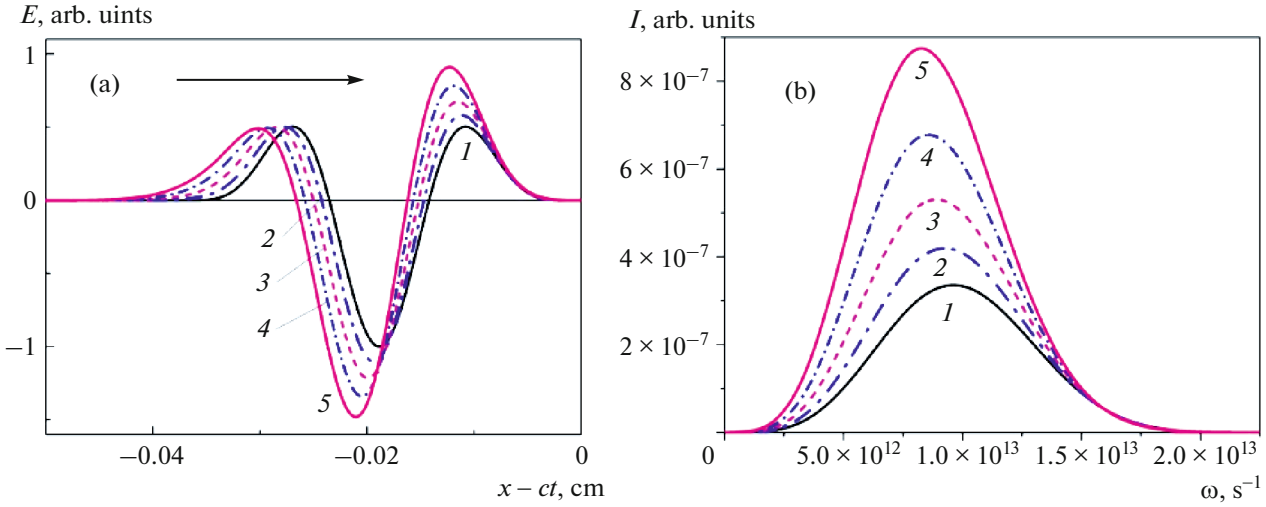

Fig. 7. (Color online) Evolution of (a) a THz pulse and (b) its central composition. The electron concentration in the plasma channel is $n_e = 3 \times 10^{13}$ cm^{-3} and the concentration of neutral particles is $N = 3 \times 10^{20}$ cm^{-3}. The arrow indicates the THz pulse propagation direction. The curves correspond to different instants: 0 (*1*), 0.25 (*2*), 0.5 (*3*), 0.75 (*4*), and 1 ns (*5*).

Let us now analyze in detail the variation of the pulse energy during the pulse propagation in the channel plasma. The corresponding data are given in Fig. 9. It can be seen that at a high gas pressure ($N = 3 \times 10^{20}$ cm^{-3}), when almost the entire frequency band of the THz signal is in the amplification zone, its energy increases approximately exponentially during the propagation in the channel. The radiation amplification factors are 0.0302 cm^{-1} and 0.117 cm^{-1} for electron concentrations $n_e = 3 \times 10^{13}$ cm^{-3} and $n_e = 10^{14}$ cm^{-3} in channels, respectively. With decreasing gas pressure, the situation becomes more complicated. An increasingly large part of the spectral composition of the pulse lies in the absorption region; as a result, its high-frequency part is absorbed (over small propagation lengths, this leads to a decrease in the pulse energy). At the same time, the low-frequency part of the pulse is amplified, which increases the total energy of the pulse when the propagation length exceeds a certain critical value. For example, for concentration $N = 10^{20}$ cm^{-3} and $n_e = 3 \times 10^{13}$ cm^{-3}, this critical length is approximately 10 cm. As noted above, the

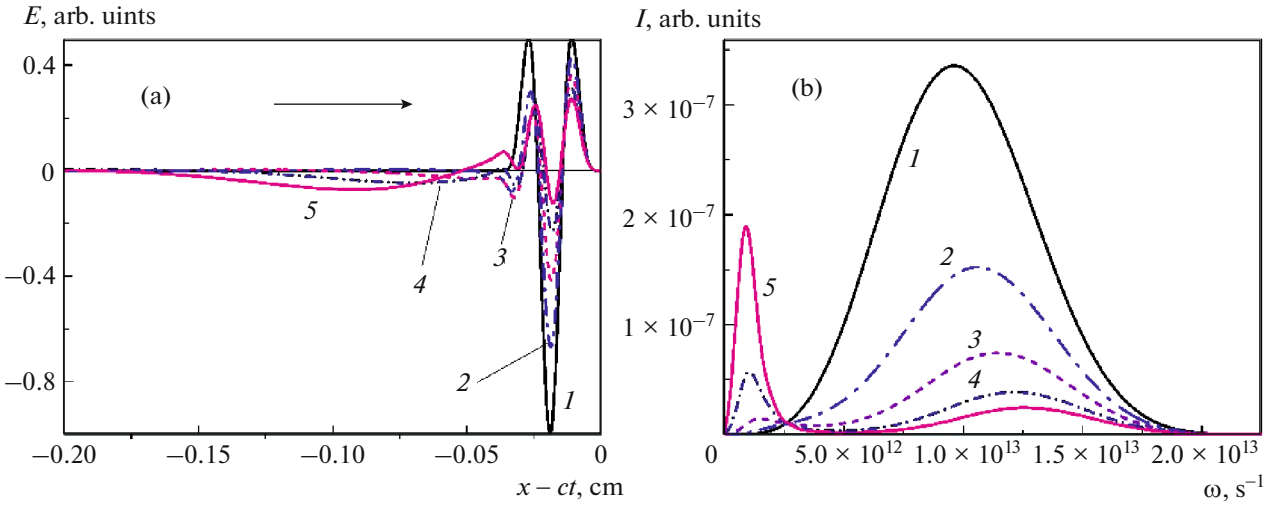

Fig. 8. (Color online) Evolution of (a) a THz pulse and (b) its central composition. The electron concentration in the plasma channel is $n_e = 3 \times 10^{13}$ cm^{-3} and the concentration of neutral particles is $N = 3 \times 10^{19}$ cm^{-3}. The arrow indicates the THz pulse propagation direction. The curves correspond to different instants: 0 (*1*), 0.1 (*2*), 0.2 (*3*), 0.3 (*4*), and 0.4 ns (*5*).

spectral composition of the pulse in such a situation "turns red," and the channel plasma can be treated as a medium transforming the radiation transmitted in it into radiation with a lower frequency. In this case, the propagating pulse itself is tailed, and the change in its energy cannot be described by an exponential law any longer.

Until now, we have considered the situation when the beginning of the leading edge of a THz pulse coincides with the position of the femtosecond laser pulse. Let us now consider the situation when a certain delay of the THz signal relative to the femtosecond UV pulse takes place. The results of calculation of the pulse amplification (the ratio of the radiation intensity over length L to the initial intensity value) in a channel of length $L = 30$ cm with gas density $N = 3 \times 10^{20}$ cm^{-3} and electron concentration $n_e = 3 \times 10^{13}$ cm^{-3} for various delay times between the UV laser pulse and terahertz pulse are shown in Fig. 10. It can be seen that as a result of rapid relaxation of the photoelectron energy spectrum as a result of vibrational excitation of nitrogen molecules for the parameters used in our calculations, the amplification of the pulse is possible only for delay times not exceeding 1 ps.

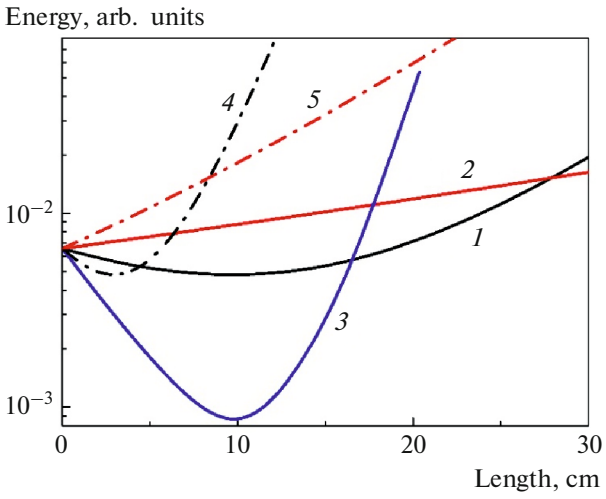

Fig. 9. (Color online) Dependence of the energy of a THz pulse propagating in a nonequilibrium plasma channel on the propagation length. Channel plasma parameters: $N = 10^{20}$ (*1*, *4*), 3×10^{20} (*2*, *5*), and 3×10^{19} cm^{-3} (*3*); electron concentration is $n_e = 3 \times 10^{13}$ (*1*–*3*) and 10^{14} cm^{-3} (*4*, *5*).

5. CONCLUSIONS

Thus, based on analysis of the second-order wave equation and the Boltzmann kinetic equation for the electron velocity distribution function, we have considered a model of propagation of an ultrashort THz pulse in a strongly nonequilibrium plasma channel formed in air by the third harmonic of a titanium–sapphire laser. The effect of amplification of the THz pulse is ensured by the formation of the photoionization peak in the electron spectrum located in the region where it increases with the transport scattering energy cross section. The model constructed in this study takes into account the time variation of the function of the response to the external THz field due to the relaxation of the electron velocity distribution function, which is determined primarily by the vibrational excitation of nitrogen molecules. In analysis of the propagation of an ultrashort laser pulse characterized by a broad spectrum, the results of analysis of the plasma response to a strong nonmonochromatic

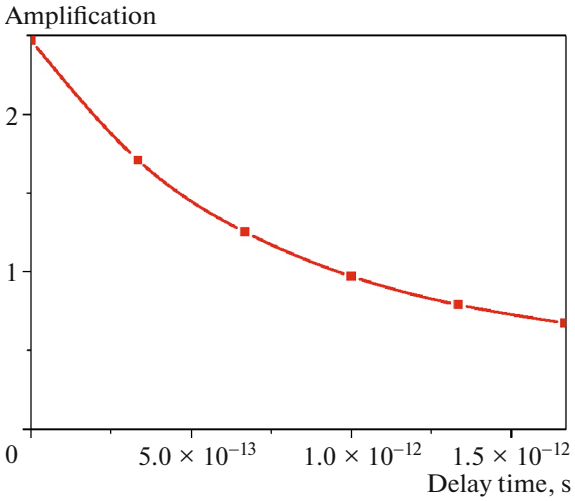

Fig. 10. (Color online) Dependence of the amplification of a THz pulse in a plasma channel of length 30 cm on the delay time between the laser and THz pulses. Calculations were made for $N = 3 \times 10^{20}$ cm^{-3} and $n_e = 3 \times 10^{13}$ cm^{-3}.

action are of fundamental importance. During the propagation of such a pulse in the channel, its energy can vary in accordance with a nonexponential law, and the absorption of the pulse energy in the channel at the initial stages can change to amplification effect over larger propagation lengths. The spectrum of the initial THz pulse can be shifted significantly towards longer wavelengths during its propagation, which considerably distorts the pulse shape and increases the pulse duration.

It is shown that at gas pressures of a few atmospheres, an order-of-magnitude amplification of the THz signal energy can be achieved over a length of 30 cm.

In this study, we have assumed that a THz pulse is quite weak and does not produce the inverse effect on the electron energy spectrum in the channel plasma. We have also confined our analysis of the wave equation to the 1D approximation. The removal of these limitations will make it possible to consider rigorously the aforementioned waveguide regime and to analyze the emerging nonlinear effects associated with the influence of the THz pulse being amplified on the kinetic processes in the plasma. Both these effects become especially important in the case of large propagation lengths.

FUNDING

This study was supported by the Russian Science Foundation (project no. 18-72-00125). Numerical calculations were performed on the Lomonosov supercomputer complex of the Moscow State University.

REFERENCES

1. M. Tonouchi, Nat. Photon. **1**, 97 (2007).
2. N. Nagai, M. Sumitomo, M. Imaizumi, and R. Fukasawa, Semicond. Sci. Technol. **21**, 201 (2006).
3. J. Liu, J. Dai, S. L. Chin, and X.-C. Zhang, Nat. Photon. **4**, 627 (2010).
4. B. M. Fischer, M. Walther, and P. U. Jepsen, Phys. Med. Biol. **47**, 38071 (2002).
5. W. H. Fan, A. Burnett, P. C. Upadhya, J. Cunningham, E. H. Linfield, and A. G. Davies, Appl. Spectrosc. **61**, 638 (2007).
6. N. Laman, S. Harsha, and D. Grischkowsky, Appl. Spectrosc. **62**, 319 (2008).
7. Y.-Ch. Shen, Int. J. Pharm. **417**, 48 (2011).
8. M. D. Mittleman, Opt. Express **26**, 9417 (2018).
9. D. J. Cook and R. M. Hochstrasser, Opt. Lett. **25**, 1210 (2000).
10. M. Kress, T. Löffler, S. Eden, M. Thomson, and H. G. Roskos, Opt. Lett. **29**, 11202 (2004).
11. K. Y. Kim, J. H. Glownia, A. J. Taylor, and G. Rodriguez, Opt. Express **15**, 4577 (2007).
12. V. Yu. Fedorov et al., Plasma Phys. Control. Fusion **59**, 014025 (2017).
13. D. Dietze, J. Darmo, S. Roither, A. Pugzlys, J. N. Heyman, and K. Unterrainer, J. Opt. Soc. Am. B **26**, 2016 (2009).
14. F. Théberge, M. Châteauneuf, G. Roy, P. Mathieu, and J. Dubois, Phys. Rev. A **81**, 033821 (2010).
15. M. Esaulkov, O. Kosareva, V. Makarov, N. Panov, and A. Shkurinov, Front. Optoelectron. **8**, 73 (2014).
16. A. A. Silaev and N. V. Vvedenskii, Phys. Rev. Lett. **102**, 115005 (2009).
17. I. Babushkin, S. Skupin, and J. Herrmann, Opt. Express **18**, 9658 (2010).
18. M. Clerici et al., Phys. Rev. Lett. **110**, 253901 (2013).
19. L. D. Landau and E. M. Lifshits, *Course of Theoretical Physics*, Vol. 8: *Electrodynamics of Continuous Media* (Nauka, Moscow, 1982; Pergamon, New York, 1984), Chap. 2, § 8.
20. K. Zhong et al., Sci. Chin. Technol. Sci. **60**, 1801 (2017).
21. T. I. Oh, Y. S. You, N. Jhajj, E. W. Rosenthal, H. M. Milchberg, and K. Y. Kim, Appl. Phys. Lett. **102**, 201113 (2013).
22. M. C. Hoffmann and J. A. Fulop, J. Phys. D: Appl. Phys. **44**, 083001 (2011).
23. D. Kuk, Y. J. Yoo, E. W. Rosenthal, N. Jhajj, N. M. Milchberg, and K. Y. Kim, Appl. Phys. Lett. **108**, 121106 (2016).
24. J. Hah, W. Jiang, Z.-H. He, J. A. Nees, B. Hou, A. J. R. Thomas, and K. Krushelnick, Opt. Express **25**, 17271 (2017).
25. A. V. Bogatskaya and A. M. Popov, JETP Lett. **97**, 388 (2013).
26. G. Bekefi, Y. L. Hirshfield, and S. C. Brown, Phys. Fluids **4**, 173 (1961).
27. F. V. Bunkin, A. E. Kazakov, and M. V. Fedorov, Sov. Phys. Usp. **15**, 416 (1972).
28. A. V. Rokhlenko, Sov. Phys. JETP **48**, 663 (1978).

29. J. M. Warman, U. Sowada, and M. P. de Haas, Phys. Rev. A **31**, 1974 (1985).
30. A. V. Bogatskaya, E. A. Volkova, and A. M. Popov, Quant. Electron. **44**, 1091 (2014).
31. V. A. Kostin, I. D. Laryushin, A. A. Silaev, and N. V. Vvedenskii, Phys. Rev. Lett. **117**, 035003 (2016).
32. V. A. Andreeva, O. G. Kosareva, N. A. Panov, et al., Phys. Rev. Lett. **116**, 063902 (2016).
33. A. V. Bogatskaya and A. M. Popov, Laser Phys. **28**, 115301 (2018).
34. A. V. Bogatskaya, E. A. Volkova, and A. M. Popov, J. Phys. D **47**, 185202 (2014).
35. A. V. Phelps, JILA Inform. Center Rep. No. 26 (Univ. of Colorado, 1985).
36. A. V. Phelps and L. C. Pitchford, Phys. Rev. A **31**, 2932 (1985).
37. V. L. Ginzburg and A. V. Gurevich, Sov. Phys. Usp. **3**, 115 (1960).
38. A. V. Bogatskaya, E. A. Volkova, and A. M. Popov, Laser Phys. Lett. **12**, 035301 (2015).
39. A. V. Bogatskaya and A. M. Popov, Laser Phys. Lett. **16**, 066008 (2019).
40. A. V. Bogatskaya, A. M. Popov, and I. V. Smetanin, J. Russ. Laser Res. **35**, 437 (2015).
41. A. V. Bogatskaya, E. A. Volkova, and A. M. Popov, Laser Phys. **29**, 086002 (2019).

Translated by N. Wadhwa